Time-Resolved Laser-Flash Photolysis Faraday Rotation Spectrometer: A New Tool for Total OH Reactivity Measurement and Free Radical Kinetics Research

Nana Wei, Bo Fang, Weixiong Zhao, Chunhui Wang, Nana Yang, Weijun Zhang, Weidong Chen, Christa Fittschen

Time-resolved laser-flash photolysis Faraday rotation spectrometer: a new tool for total OH reactivity measurement and free radical kinetics research

Nana Wei, [†,‡] Bo Fang, [†,‡] Weixiong Zhao, [*,†] Chunhui Wang, [†,‡] Nana Yang, [†,‡] Weijun Zhang, [*,†,‡] Weidong Chen, [§] Christa Fittschen [//]

[†] Laboratory of Atmospheric Physico-Chemistry, Anhui Institute of Optics and Fine Mechanics, Chinese Academy of Sciences, Hefei 230031, Anhui, China

[‡] University of Science and Technology of China, Hefei 230026, Anhui, China

[§] Laboratoire de Physicochimie de l'Atmosphère, Université du Littoral Côte d'Opale, 59140 Dunkerque, France

[//] Université Lille, CNRS, UMR 8522 - PC2A -Physicochimie des Processus de Combustion et de l'Atmosphère, F-59000 Lille, France

ABSTRACT: The total OH reactivity (k'_{OH}) is an important parameter for quantitative assessment of the atmospheric oxidation capacity. Although laboratory measurement of k'_{OH} has been achieved 20 years ago, the instruments required are often costly and complex. Long-term atmospheric observations remain challenging and elusive. In this work, a novel instrument combining laser-flash photolysis with a mid-infrared Faraday rotation spectrometer (LFP-FRS) has been developed for the measurement of k'_{OH} and for studying gas phase free radical kinetics. The reactor is composed of a Herriott-type optical multipass cell, and OH radicals were generated by flash photolysis of ozone with a 266 nm pulsed Nd:YAG laser. The decay of the OH signal was directly measured with a time-resolved FRS spectrometer at 2.8 μm. The overlapping pathlength between the pump beam and probe beam was 25 m. Increased performance was achieved by subtracting the signals before and after flash photolysis to eliminate interferences caused by H_2O absorption and background drift. The optimum precisions (1σ) of OH concentration and k'_{OH} measurement were 4×10^6 molecule cm^{-3} and 0.09 s^{-1} over data acquisition times of 56 s and 112 s, respectively. The performance of the system was evaluated by the reaction of OH with CO and NO. The measured rate coefficients (k_{OH+CO} and k_{OH+NO}) were in good agreement with values reported in the literature. The developed LFP-FRS provides a new, high precision, and highly selective tool for atmospheric chemistry research of OH radicals and other transient paramagnetic free radicals such as HO_2 radicals.

The total OH reactivity (k'_{OH}) is equal to the reciprocal of the atmospheric lifetime of OH (τ_{OH}), and is an important parameter for quantitative assessment of the atmospheric oxidation capacity. It is defined as the total pseudo-first-order loss rate of OH in ambient air caused by the reactions of OH with most pollutants and greenhouse gases, such as volatile organic compounds (VOCs), CO, NO_x (= NO+NO_2), CH_4, etc., [1-4]

$$k'_{OH} = \sum k_{OH+X_i}[X_i] = \tau_{OH}^{-1} \quad (1)$$

where X_i represents the reactive species with concentration $[X_i]$. k_{OH+Xi} is the reaction rate coefficient of OH with each species. Due to its high reactivity and short life time, the production (P_{OH}) and sink ($k'_{OH}[OH]$) of atmospheric OH radicals can be described by steady-state equation: [2,3,5]

$$\frac{d[OH]}{dt} = P_{OH} - k'_{OH}[OH] = 0. \quad (2)$$

Therefore, measurement of k'_{OH} in combination with OH concentration ([OH]) provides insight into OH production and loss processes and is a powerful test of our understanding of atmospheric oxidation chemistry. [6-8]

There are two common ambient k'_{OH} measurement methods, the essence of which is the measurement of free radical kinetics. [9-12] The first is to measure the OH decays directly with the laser-induced fluorescence spectroscopy (LIF) [1-5] or semi-directly with chemical ionization mass spectrometry (CIMS) [13]. High concentrations of OH radicals are artificially generated either by laser-flash photolysis (LFP) of O_3 with a 266 nm laser pulse (pulsed pump-probe) [2-4] or by continuous photolysis of H_2O at 184.9 nm with a mercury lamp in a flow tube (FT) [1,5,13,14]. The second method is the comparative reactivity method (CRM) based on competitive kinetics. A non-ambient reactive VOC (reference reagent such as pyrrole, C_4H_5N) is introduced into the glass reactor. The loss of OH is measured by detecting changes in the concentration of the reference reagent either in zero air or in ambient air with proton transfer reaction mass spectrometer (PTR-MS) or gas chromatographic photoionization detector (GC-PID).[15,16]

While k'_{OH} was first measured in the laboratory 20 years ago,[9,17] the necessary instrumentation is costly and complex. Only a few research groups can make such measurements.[3,12,18] The long-term observation of k'_{OH} and k'_{OH} as a

standard feature of atmospheric observations therefore remains challenging and elusive. [9]

In this work, we report the development of a new instrument that combines laser-flash photolysis with mid-infrared Faraday rotation spectroscopy (LFP-FRS) for real-time in-situ measurement of k'_{OH} and free radical kinetics studies. The OH decay was directly measured using a time-resolved FRS spectrometer at 2.8 μm. [19-21] FRS is based on the magneto-optic effect of paramagnetic species, which provides a powerful tool for gas phase chemical kinetic studies with high precision, high selectivity, and free of interferences from precursor's absorption. [22-25] Further improvements can make the system more compact, portable, and affordable, which provides a reliable approach for long-term and network k'_{OH} observations.

EXPERIMENTAL SECTION

The experimental setup of the LFP-FRS instrument is shown in Figure 1. The instrument consists of two parts: an FRS spectrometer for real-time in-situ measurement of OH radicals and a LFP device for generating pulses of high concentrations (~ 10^9 molecule/cm^3) of OH radicals.

The probe laser of the FRS spectrometer was a 2.8 μm continuous-wave (CW) distributed feedback (DFB) diode laser controlled by a LDC501 controller (Stanford Research). The Q(1.5e) line of the $^2\Pi_{3/2}$ state at 3568.5238 cm^{-1}, with the strongest line absorption intensity (9.556×10^{-20} cm^{-1}/(molecule cm^{-2})) and the largest effective g_J (the rotational gyromagnetic ratio) value (0.936) in the infrared region, was chosen as the best probe for OH detection. [19] Wavelength modulation spectroscopy (WMS) combined with a static magnetic field (DC-field) was used to efficiently modulate the Zeeman splitting of the absorption line. [20] The laser frequency was tuned in two ways: [21] (1) a point-by-point tuning method, using a GPIB card to control the laser injection current at each step; (2) a wavelength sweeping method, scanning the laser injection current with a continuous ramp provided by a function generator. For WMS detection, a sinusoidal modulation with a frequency (f_m) of 50 kHz from a lock-in amplifier (SR865, Stanford Research) was added to the injection current. The signal detected by the detector is demodulated (second-harmonic, 2f detection) by the lock-in amplifier with a time constant of 300 μs to obtain the FRS signal. For weak absorptions, the FRS signal is proportional to the radical concentration (N) and absorption pathlength (L):[19-21]

$$FRS(\nu) = N \times S \times L \times \sin 2\varphi \times \chi(\nu), \qquad (3)$$

where ν is the frequency, S is the absorption line intensity, φ is the offset angle of the two polarizer, and $\chi(\nu)$ is the lineshape function.

To increase the length of the absorption path and thus improve the detection precision and sensitivity, a Herriott-type optical multipass cell [26,27] was used. The cell was also used as the reactor for flash photolysis. The collimated beam from the probe laser was first passed through a polarizer (Rochon prism) to clean up the polarization state and then directed into the Herriott cell. Light transmitted through the optical cell passed through a second Rochon prism (polarization analyzer) to a thermoelectrically cooled detector. The analyzer's purpose was to reduce the laser noise and thereby increase the signal-to-noise ratio (SNR) of the system. [19,24,28] The polarization axis of the analyzer was typically set at a small offset angle to the orthogonal axis of the polarization axis of the first polarizer. In this work, the maximum SNR was achieved at an offset angle of φ = 7º.

The Herriott cell consisted of two spherical mirrors with a radius of curvature of 1300 mm and a diameter of 50 mm. In the center of the mirror was a 32 mm in diameter hole for the laser photolysis beam. At the edge of the mirror was a 5 mm diameter hole for the coupling of the probe laser. The flash laser beam (266 nm, 25 mJ, 8 ns pulse duration) from a compact pulsed Nd:YAG laser (Ultra 100, Quantel laser) was expanded to a diameter of 30 mm with a beam expander. The base length of the Herriott cell was 1220 mm. The total optical pathlength was 60 m from 49 back and forth reflections (25 spots on the mirror, as shown in Figure 1). The overlap distance between the photolysis beam and the probe beam was estimated to be 25 m by ray-tracing software. On the outside of the Herriott cell, an 800 mm long water-cooled solenoid with an inner diameter of 62 mm was placed. The coil was made of 1 mm diameter enamel-coated copper wire. The magnetic field strength (B) was adjustable (~ 40 Gauss/A) by changing the coil current. The pressure and temperature inside the reactor were controlled at 50 mbar and 28 ºC, respectively.

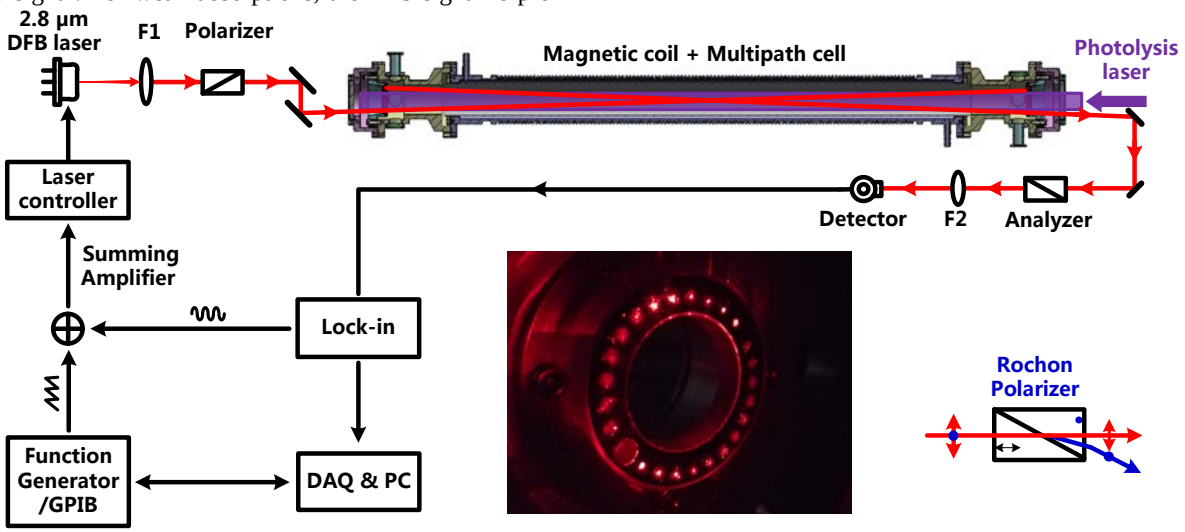

Figure 1. A schematic of the LFP-FRS system and a photograph of the light spot pattern in the Herriott-type multipass cell. Both the polarizer and the analyzer used were Rochon type prisms. F: lens, DAQ: data acquisition, PC: personal computer.

A small amount of the zero air (with a flow rate of 0.2 L/min) was bypassed through an ozone generator before being added to the sample (with a flow rate of 1 L/min) to obtain an O_3 concentration of ~ 1.5×10^{12} molecule/cm^3 in the reactor.[18] Like the LFP-LIF instrument used for k'_{OH} measurement, OH radicals in the reactor were generated by photolysis of O_3 at 266 nm in the presence of H_2O:[29,30]

$$O_3 + h\nu\ (266\ \text{nm}) \rightarrow O(^1D) + O_2, \quad (4)$$

$$O(^1D) + M \rightarrow O(^3P) + M, \quad (5)$$

$$O(^1D) + H_2O \rightarrow 2OH, \quad (6)$$

where M is the inert "bath" gas such as N_2 or O_2. The recommend quantum yield of excited singlet oxygen atom $O(^1D)$ produced by O_3 photolysis is 0.90±0.05.[31] Under the current experimental condition, about less than 5% O_3 can be photolyzed, resulting in ~ 6.8×10^{10} molecule/cm^3 of $O(^1D)$ in the reactor. Once an $O(^1D)$ is formed, it is either quenched to its ground-state ($O(^3P)$) or reacts with H_2O to generate OH radicals. $O(^3P)$ will rapidly react with O_2 to produce O_3:

$$O(^3P) + O_2 + M \rightarrow O_3 + M. \quad (7)$$

The number of OH radicals produced by each $O(^1D)$ is:[30]

$$\varepsilon_{OH} = \frac{2k_6[O(^1D)][H_2O]}{(k_5[M]+k_6[H_2O])[O(^1D)]} \cong \frac{2k_6}{k_5}\xi_{H_2O}, \quad (8)$$

where k_5 and k_6 are the rate coefficients for reactions (5) and (6). [$O(^1D)$], [H_2O], and [M] are the concentrations of the corresponding molecule. ξ_{H_2O} is the mixing ratio of H_2O. At 298 K, k_5 is 2.9×10^{-11} cm^3 molecule^{-1} s^{-1} for the atmospheric N_2/O_2 mixing ratio, and k_6 is 2.2×10^{-10} cm^3 molecule^{-1} s^{-1}.[30,31] The concentration of OH produced in the reactor depends on the mixing ratio of H_2O. When ξ_{H_2O} was ~ 0.2% ([H_2O] ~ 3×10^{15} molecule/cm^3 at 50 mbar), the concentration of OH radicals that can be generated in the reactor was ~ 2×10^9 molecule/cm^3.

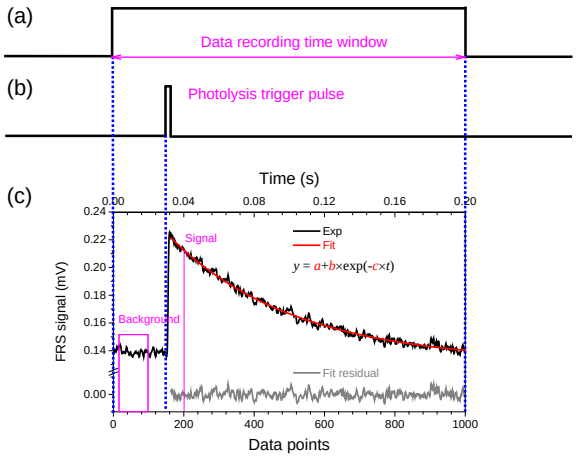

Figure 2. Timing scheme of data acquisition and laser photolysis for one laser photolysis pulse. (a) TTL signal generated by function generator for DAQ card data acquisition. Data record begins to record from the rising edge of the TTL and ends at the end of the falling edge. (b) Delayed pulse generated by a digital delay generator for triggering photolysis pulse. (c) Experimental time-resolved FRS signal for OH decay (average signal of 40 pulses), exponential fit and the corresponding fit residual.

The pulse repetition rate of the flash photolysis laser ranged from 1 to 5 Hz. The corresponding data acquisition and triggering scheme is shown in Figure 2. The rising edge of the TTL signal generated by the function generator (Figure 2(a)) was used to trigger the data acquisition of the DAQ card. The delayed pulse generated by DG645 digital delay generator (Stanford Research) was used to trigger the photolysis laser.[32] The signal acquired between the two rising edges was the background signal without photolysis. When the pulsed laser was triggered, O_3 was photolyzed and reacted rapidly with H_2O to produce OH radicals. The FRS signal increased rapidly. The OH decay was fitted with a single-exponential equation:

$$[OH] = [OH]_0 \exp(-k'_{OH}\, t), \quad (9)$$

to get the total reactivity k'_{OH} and the reaction rate associated with the OH radical. An example of the fitting result and the corresponding residual is shown in Figure 2(c).

RESULTS AND DISCUSSION

Unlike the commonly used differential detection scheme with two detectors,[20,33,34] or the method of subtracting the zero air signal from the sample signal by quickly flushing the absorption cell,[35] a special background subtraction technique was used in this work. Figure 3 shows an example of the data processing method to get the FRS 2*f* signal of the OH absorption. We used the average value over ca. 0.02 s (marked with a magenta box in Figure 2(c)) before laser photolysis for the background signal, and a fixed time point (marked with a magenta line in Figure 2(c)) shortly after the photolysis as the sample signal (as shown in Figure 3(a)). By subtracting the background from the signal, the adjacent H_2O absorption and baseline drift of the 2*f* signal were completely eliminated, and the FRS signal of OH absorption can be clearly observed (Figure 3(b)). This method strongly suppressed laser noise, optical interference, and the absorption of the precursor, allowing the instrument to achieve a very high performance.

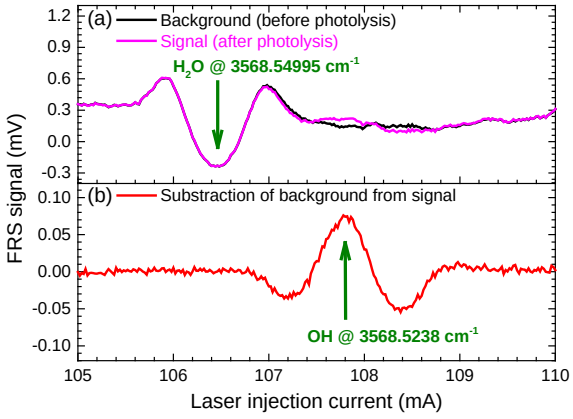

Figure 3. (a) FRS 2*f* signals (40 pulses average) before (black line, no OH absorption, used as background signal) and after (magenta line, with OH absorption) laser photolysis. (b) OH signal. After subtracting the background from the signal, the absorption of OH was clearly observed ([OH] ~ 4×10^8 molecule/cm^3). This method effectively eliminated the influence of H_2O absorption and baseline drift. The point-by-point method was used for the laser wavelength tuning.

The OH concentration in the reactor was determined by the WMS 2*f* detection scheme. The WMS 2*f* signal (B = 0) of OH absorption was obtained using the same method as FRS 2*f* signal. H_2O (absorption at 3568.54995 cm^{-1}) with known concentration (determined from direct absorption) was used as the reference for the cross-calibration of the OH concentration (absorption at 3568.5238 cm^{-1}). Details can be found in our previous work.[19,20] The total uncertainty in OH concentration determination was estimated to be < 5%.[20] The relationship between the peak intensities of FRS 2*f* signals and OH concentrations is shown in Figure 4. The FRS signal was linearly proportional to the OH concentrations with a fit uncertainty of less than 1%: [OH] (molecule/cm^3) = 2.23(±5.08)×10^6 (molecule/cm^3) + 5.39(±0.05) ×10^9 (molecule/cm^3/mV) × FRS signal (mV). The 1 mV FRS signal corresponded to an OH concentration of 5.39×10^9 molecule/cm^3.

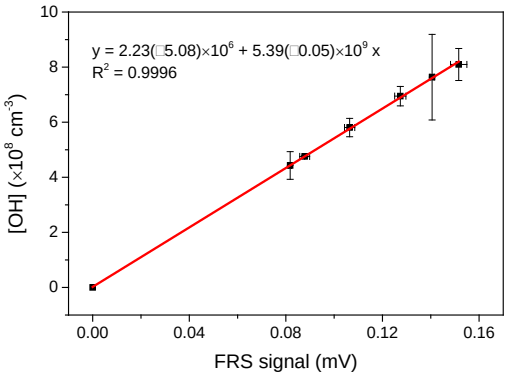

Figure 4. The linear relationship between the measured peak intensities of the FRS 2*f* signals and the OH concentrations.

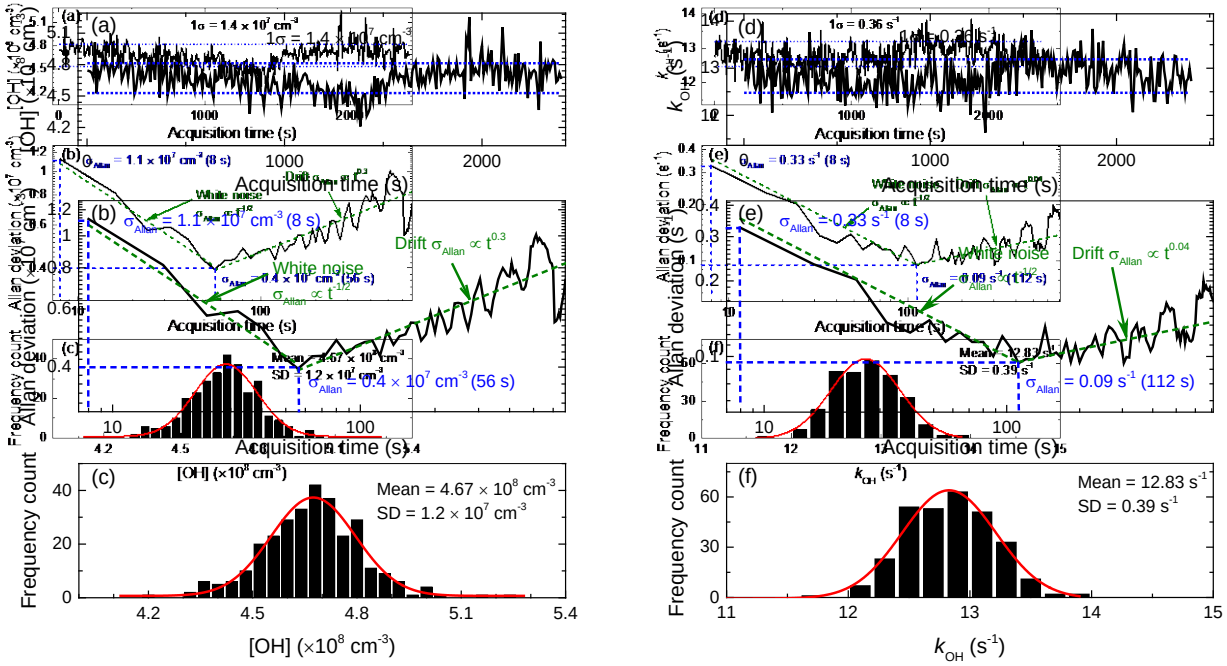

Figure 5. Performance evaluation of the LFP-FRS instrument for [OH] (a-c) and k'_{OH} (d-f) measurements with zero air. Upper panel: time series measurement of (a) [OH] and (d) k'_{OH}. Middle panel: Allan deviation plots for (b) [OH] and (e) k'_{OH}. The dominant regions of white noise ($\sigma_{Allan} \propto t^{-1/2}$) and drift ($\sigma_{Allan} \propto t^{\alpha}$, α = 0.3 and 0.04) are shown as the olive dashed lines. Lower panel: frequency distribution of the corresponding time series measurement of (c) [OH] and (f) k'_{OH}.

The precisions of the LFP-FRS instrument for OH concentration and k'_{OH} measurements were evaluated with Allan variance analysis (Figure 5).[36] The upper panels of Figure 5 show a 40 minutes continuous measurement of [OH] and k'_{OH} by photolysis of the mixture of zero air and O_3. The pressure inside the reactor was maintained at 50 mbar. Forty decays (with 5 Hz pulse repetition rate) were averaged (with an 8 s total acquisition time) for data analysis. [OH] was calculated using the FRS 2*f* signal intensities at a fixed time point (10 ms after photolysis) with the linear relationship obtained in Figure 4. k'_{OH} was obtained directly by exponential fitting of the averaged decay. The corresponding frequency distribution plot of the time series measurement of [OH] and k'_{OH} are shown in the lower panel.

The Allan variance analysis (middle panel of Figure 5) shows that the precision of OH concentration measurements was about 1.1×10^7 molecule/cm^3 over 8 s integration time, and can be further improved to 4×10^6 molecule/cm^3 over 56 s integration time. For k'_{OH}, measurement precisions were 0.33 s^{-1} and 0.09 s^{-1} over 8 s and 112 s, respectively. For ambient applications, a correction of the pressure is necessary to get the actual OH decay rate. By pumping the ambient air sample (1 atm) into the reactor (50 mbar), the concentration of the reactant was decreased by ~ 20 times, and the corresponding reactivity was also roughly reduced by ~ 20 times (in simple terms). The achievable precision of the developed LFP-FRS for ambient k'_{OH} measurement was therefore estimated to be ~ 1.8 s^{-1}. This precision is favorably compared to state-of-the-art

LIF instruments.[18] By increasing the pressure in the reactor, this limit can be further reduced.

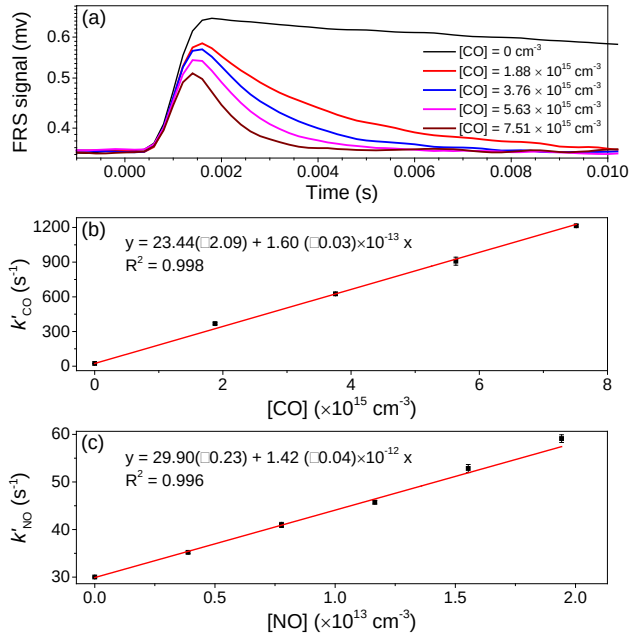

Figure 6. (a) Examples of the measured OH decay FRS signals of zero air and different concentrations of CO, and a plot of the pseudo-first-order decay rates versus reactant concentration: (b) CO and (c) NO. The laser frequency was fixed at the peak position of the OH absorption.

The accuracy of the measured OH decay rate with the developed LFP-FRS instrument was evaluated with the well-known reactions of OH with CO and NO. Taking the CO reaction as an example to illustrate the verification process, the measured OH decay signals for zero air and different concentrations of CO are shown in Figure 6(a), which satisfied the following equation:

$$\frac{d[\mathrm{OH}]}{dt} = -k'_{\mathrm{CO}}[\mathrm{OH}] = -k_{\mathrm{OH+CO}}[\mathrm{CO}][\mathrm{OH}] \quad (10)$$

where k'_{CO} is the pseudo-first order rate constant of the OH reaction with CO obtained from the exponential fitting, and k_{OH+CO} is the reaction rate constant of OH with CO. k'_{CO} increased as the reactant concentration increased. The slope of the measured k'_{CO} versus CO concentration (absolute concentration at 50 mbar and 28 ºC) represents the reaction rate constant k_{OH+CO} (as shown in Figure 6(b)). For CO, the measured rate constants was 1.60 (±0.03)×10^{-13} cm^3 $molecule^{-1}$ s^{-1}, in good agreement with the IUPAC (International Union of Pure and Applied Chemistry) preferred value (~ 1.48×10^{-13} cm^3 $molecule^{-1}$ s^{-1}).[37] For NO (as shown in Figure 6(c)), the measured rate was 1.42 (±0.04)×10^{-12} cm^3 $molecule^{-1}$ s^{-1}, which also agreed with literature values (ranging from 8.45×10^{-13} – 1.34×10^{-12} cm^3 $molecule^{-1}$ s^{-1}).[31]

The fitted intercepts in Figure 6(b) and (c) represent the non-reactive loss of OH to wall losses and diffusion losses, depending on experimental conditions. By frequently recording and subtracting k'_{OH} in zero air, the effect of the non-reactive loss and the intercept changes can be effectively avoided. The developed LFP-FRS instrument has been successfully applied for the first time during a field campaign carried out on the Tibet Plateau during the period of May to July 2019. The total OH reactivity of the Namucuo area (4730 m above sea level) has been obtained. The relevant results will be reported in subsequent articles.

CONCLUSIONS

In this work, we report the development of a novel method that combines laser-flash photolysis with mid-infrared Faraday rotation spectroscopy for k'_{OH} measurement and gas phase radical kinetics studies. By performing background subtraction of the signal before laser photolysis, influence of laser noise, optical interference, and precursor's absorption on the signal could be greatly reduced, and high performance was achieved. The optimized detection precisions that could be achieved were 4×10^6 molecule/cm^3 and 0.09 s^{-1} for OH concentration and k'_{OH} measurement with 56 s and 112 s integration time, respectively, with an effective absorption pathlength of 25 m.

The instrument described here provides a new, high precision, and highly selective tool for radical chemistry research. It is not only applicable to the OH radical and can be extended to other transient paramagnetic free radicals such as the HO_2 radical.[25,38] With the rapid development of laser, detector, and electronics, this laser spectroscopy instrument can be made more compact and affordable. This work provides a reliable method with low maintenance cost for field k'_{OH} applications. Further improvements will make long-term and network observations possible.

AUTHOR INFORMATION

Corresponding Author

* Tel.: +86-551-65591961; Fax: +86-551-65591560; E-mail: wxzhao@aiofm.ac.cn (W. Zhao)
* E-mail: wjzhang@aiofm.ac.cn (W. Zhang).

ORCID

Weixiong Zhao: 0000-0003-1700-8992
Christa Fittschen: 0000-0003-0932-432X

Notes

The authors declare no competing financial interest.

ACKNOWLEDGMENT

This research is supported by the National Natural Science Foundation of China (41627810, 91544228), the Instrument Developing Project of the Chinese Academy of Sciences (YZ201626), the Youth Innovation Promotion Association CAS (2016383), the CASHIPS Director's Fund (BJPY2019B02, YZJJ2018QN7), and the CAS President's International Fellowship Initiative (PIFI) project. We thank Dean Venables for his comments on the paper.

REFERENCES

(1) Kovacs, T. A.; Brune, W. H. *J. Atmos. Chem.* **2001,** 39, 105-122.

(2) Sadanaga, Y.; Yoshino, A.; Watanabe, K.; Yoshioka, A.; Wakazono, Y.; Kanaya, Y.; Kajii, Y. *Rev. Sci. Instrum.* **2004,** 75, 2648-2655.

(3) Lou, S.; Holland, F.; Rohrer, F.; Lu, K.; Bohn, B.; Brauers, T.; Chang, C. C.; Fuchs, H.; Häseler, R.; Kita, K.; Kondo, Y.; Li, X.; Shao, M.; Zeng, L.; Wahner, A.; Zhang, Y.; Wang, W.; Hofzumahaus, A. *Atmos. Chem. Phys.* **2010,** 10, 11243-11260.

(4) Stone, D.; Whalley, L. K.; Ingham, T.; Edwards, P. M.; Cryer, D. R.; Brumby, C. A.; Seakins, P. W.; Heard, D. E. *Atmos. Meas. Tech.* **2016,** 9, 2827-2844.

(5) Ingham, T.; Goddard, A.; Whalley, L. K.; Furneaux, K. L.; Edwards, P. M.; Seal, C. P.; Self, D. E.; Johnson, G. P.; Read, K. A.; Lee, J. D.; Heard, D. E. *Atmos. Meas. Tech.* **2009,** 2, 465-477.

(6) Di Carlo, P.; Brune, W. H.; Martinez, M.; Harder, H.; Lesher, R.; Ren, X. R.; Thornberry, T.; Carroll, M. A.; Young, V.; Shepson, P. B.; Riemer, D.; Apel, E.; Colleen Campbell, C. *Science* **2004,** 304, 722-725.

(7) Lelieveld, J.; Butler, T. M.; Crowley, J. N.; Dillon, T. J.; Fischer, H.; Ganzeveld, L.; Harder, H.; Lawrence, M. G.; Martinez, M.; Taraborrelli, D.; Williams, J. *Nature* **2008,** 452, 737-740.

(8) Hofzumahaus, A.; Rohrer, F.; Lu, K.; Bohn, B.; Brauers, T.; Chang, C.-C.; Fuchs, H.; Holland, F.; Kita, K.; Kondo, Y.; Li, X.; Lou, S.; Shao, M.; Zeng, L.; Wahner, A.; Zhang, Y. *Science* **2009,** 324, 1702-1704.

(9) Williams, J.; Brune, W. *Atmos. Environ.* **2015,** 106, 371-372.

(10) Yang, Y.; Shao, M.; Wang, X.; Nölscher, A. C.; Kessel, S.; Guenther, A.; Williams, J. *Atmos. Environ.* **2016,** 134, 147-161.

(11) Yang, X.; Wang, H.; Tan, Z.; Lu, K.; Zhang, Y. *Acta Chim. Sinica* **2019,** 77, 613-624.

(12) Fuchs, H.; Novelli, A.; Rolletter, M.; Hofzumahaus, A.; Pfannerstill, E. Y.; Kessel, S.; Edtbauer, A.; Williams, J.; Michoud, V.; Dusanter, S.; Locoge, N.; Zannoni, N.; Gros, V.; Truong, F.; Sarda-Esteve, R.; Cryer, D. R.; Brumby, C. A.; Whalley, L. K.; Stone, D.; Seakins, P. W.; Heard, D. E.; Schoemaecker, C.; Blocquet, M.; Coudert, S.; Batut, S.; Fittschen, C.; Thames, A. B.; Brune, W. H.; Ernest, C.; Harder, H.; Muller, J. B. A.; Elste, T.; Kubistin, D.; Andres, S.; Bohn, B.; Hohaus, T.; Holland, F.; Li, X.; Rohrer, F.; Kiendler-Scharr, A.; Tillmann, R.; Wegener, R.; Yu, Z.; Zou, Q.; Wahner, A. *Atmos. Meas. Tech.* **2017,** 10, 4023 - 4053.

(13) Muller, J. B. A.; Elste, T.; Plass-Dülmer, C.; Stange, G.; Holla, R.; Claude, A.; Englert, J.; Gilge, S.; Kubistin, D. *Atmos. Meas. Tech.* **2018,** 11, 4413-4433.

(14) Mao, J.; Ren, X.; Brune, W. H.; Olson, J. R.; Crawford, J. H.; Fried, A.; Huey, L. G.; Cohen, R. C.; Heikes, B.; Singh, H. B.; Blake, D. R.; Sachse, G. W.; Diskin, G. S.; Hall, S. R.; Shetter, R. E. *Atmos. Chem. Phys.* **2009,** 9, 163-173.

(15) Sinha, V.; Williams, J.; Crowley, J. N.; Lelieveld, J. *Atmos. Chem. Phys.* **2008,** 8, 2213-2227.

(16) Nolscher, A. C.; Sinha, V.; Bockisch, S.; Klupfel, T.; Williams, J. *Atmos. Meas. Tech.* **2012,** 5, 2981-2992.

(17) Calpini, B.; Jeanneret, F.; Bourqui, M.; Clappier, A.; Vajtai, R.; van den Bergh, H. *Analusis* **1999,** 27, 328-336.

(18) Hansen, R. F.; Blocquet, M.; Schoemaecker, C.; Léonardis, T.; Locoge, N.; Fittschen, C.; Hanoune, B.; Stevens, P. S.; Sinha, V.; Dusanter, S. *Atmos. Meas. Tech.* **2015,** 8, 4243 - 4264.

(19) Zhao, W.; Wysocki, G.; Chen, W.; Fertein, E.; Le Coq, D.; Petitprez, D.; Zhang, W. *Opt. Express* **2011,** 19, 2493-2501.

(20) Zhao, W.; Fang, B.; Lin, X.; Gai, Y.; Zhang, W.; Chen, W.; Chen, Z.; Zhang, H.; Chen, W. *Anal. Chem.* **2018,** 90, 3958-3964.

(21) Zhao, W.; Wysocki, G.; Chen, W.; Zhang, W. *Appl. Phys. B* **2012,** 109, 511-519.

(22) Adams, H.; Hall, J. L.; Russell, L. A.; Kasper, J. V. V.; Tittel, F. K.; Curl, R. F. *J. Opt. Soc. Am. B* **1985,** 2, 776-780.

(23) Blake, T. A.; Chackerian, C.; Podolske, J. R. *Appl. Opt.* **1996,** 35, 973-985.

(24) Lewicki, R.; Doty, J. H., III; Curl, R. F.; Tittel, F. K.; Wysocki, G. *Proc. Natl. Acad. Sci. U. S. A.* **2009,** 106, 12587-12592.

(25) Brumfield, B.; Sun, W.; Ju, Y.; Wysocki, G. *J. Phys. Chem. Lett.* **2013,** 4, 872-876.

(26) Pilgrim, J. S.; Jennings, R. T.; Taatjes, C. A. *Rev. Sci. Instrum.* **1997,** 68, 1875-1878.

(27) Cui, R.; Dong, L.; Wu, H.; Li, S.; Zhang, L.; Ma, W.; Yin, W.; Xiao, L.; Jia, S.; Tittel, F. K. *Opt. Express* **2018,** 26, 24318-24328.

(28) Zhao, W.; Deng, L.; Xu, X.; Chen, W.; Gao, X.; Huang, W.; Zhang, W. Proceedings of Imaging and Applied Optics 2014, Seattle, WA, U.S.A., July 13−17, 2014; The Optical Society, 2014: paper JTu4A.31.

(29) *Chemistry of the Upper and Lower Atmosphere: Theory, Experiments, and Applications;* Finlayson-Pitts, B. J., Pitts, J. N.; Academic Press, 2000; pp 130-134.

(30) *Atmospheric chemistry and physics: from air pollution to climate change;* Seinfeld, J. H., Pandis, S. N.; John Wiley & Sons, Inc., 2006; pp 205-209.

(31) Atkinson, R.; Baulch, D. L.; Cox, R. A.; Crowley, J. N.; Hampson, R. F.; Hynes, R. G.; Jenkin, M. E.; Rossi, M. J.; Troe, J. *Atmos. Chem. Phys.* **2004,** 4, 1461-1738.

(32) Thiébaud, J.; Fittschen, C. *Appl. Phys. B* **2006,** 85, 383-389.

(33) Adams, H.; Reinert, D.; Kalkert, P.; Urban, W. *Appl. Phys. B* **1984,** 34, 179-185.

(34) Brumfield, B.; Wysocki, G. *Opt. Express* **2012,** 20, 29727-29742.

(35) Fried, A.; Henry, B.; Wert, B.; Sewell, S.; Drummond, J. R. *Appl. Phys. B* **1998,** 67, 317-330.

(36) Fang, B.; Zhao, W.; Xu, X.; Zhou, J.: Ma, X.; Wang, S.; Zhang, W.; Venables, D. S.; Chen, W. *Opt. Express* **2017,** 25, 26910-26922.

(37) Atkinson, R.; Baulch, D. L.; Cox, R. A.; Crowley, J. N.; Hampson, R. F.; Hynes, R. G.; Jenkin, M. E.; Rossi, M. J.; Troe, J.; IUPAC Subcommittee. *Atmos. Chem. Phys.* **2006,** 6, 3625-4055.

(38) Miyazaki, K.; Nakashima, Y.; Schoemaecker, C.; Fittschen, C.; Kajii, Y. *Rev. Sci. Instrum.* **2013,** 84, 076106.

Figure for TOC only